Site-Selective Spectroscopy of the Solid-State Defect Chemistry in Erbium-Doped Barium Titanate

John D. Bak and John C. Wright*

Department of Chemistry, University of Wisconsin−Madison, Madison, Wisconsin 53706

Received: June 7, 2005; In Final Form: August 4, 2005

Erbium-doped barium titanate crystals were studied by laser-induced fluorescence spectroscopy. Thirteen spectroscopically distinct erbium ion sites were found. The relative concentrations of the different sites changed as a function of the crystal and its preparation and treatment. One major site was present in all crystals. The site distribution was changed either by growing codoped crystals with donor (La^{3+}) and acceptor (Sc^{3+}) ions or by changing the temperature and partial pressure of the oxygen in the annealing atmosphere. Equilibrium calculations were done to simulate the defect distributions that result from the charge compensation of the erbium ions. Comparison with the observed dependence of the site spectral intensities indicated that the erbium enters the lattice on barium sites. We assigned the dominant site to an erbium ion on a barium site that is locally compensated by a barium vacancy, whereas the other lower-intensity sites corresponded to erbium ions that are locally compensated by an electron and a more complex center of an erbium, a barium vacancy, and a hole. The spectra of one sample showed that its defects were different and were characteristic of a sample that had not equilibrated. The new sites in this sample were assigned to erbium entering the lattice on a titanium site, which was then locally compensated by an oxygen vacancy or a hole. Heating equilibrated the sample and changed the erbium to a barium site.

Introduction

A material's solid-state defect chemistry is responsible for many of its electrical, optical, chemical, and transport properties.[1,2] The defect chemistry of perovskites and related oxide materials is particularly complex because of the many possible point defect structures. Likewise, they have a wide range of properties, many of which have important technological applications. Previous work in fluorite materials has shown that the selective laser excitation of fluorescent charge-compensated lanthanide ions probes the defect chemistry of a material.[3] The probe ion's spectra reflect the local crystal fields created by the compensating defect; therefore, different defect centers produce characteristic probe ion spectra. Site-selective spectroscopy allows one to use the probe ion spectra to resolve the defect center distributions defined by the point defect equilibria, even for complex materials with many different defect centers. Because these experiments do not probe transport properties, site-selective spectroscopy can define the defect distribution at low temperatures where defects are immobile. This approach provides a "signature" for the individual defect structures that define the bulk properties of the material and allows one to follow the detailed changes in the defect distribution as it changes during crystal treatments.

Because site-selective laser spectroscopy can measure the defect equilibria in complex samples, there is interest in extending site-selective methods to the perovskites. Previous work has examined strontium titanate.[4−7] In Er^{3+}:$SrTiO_3$, the spectra depend strongly upon the Sr/Ti ratio and reflect the changing contributions from different phases because $SrTiO_3$ forms shear structures containing the Sr_2TiO_4 and $Sr_3Ti_2O_7$ phases.[6,7] In this paper, we find a very different behavior in the site-selective spectroscopy of Er^{3+}:$BaTiO_3$. We identify 13 spectroscopically distinct erbium sites that correspond to sites that are locally charge compensated by intrinsic defects, and we measure how they change as a function of annealing temperature and time, oxygen partial pressure, and acceptor and donor dopant concentrations. None of the sites correspond to other phases, such as those found in the barium oxide-rich Ba_2TiO_4 phase, the titanium dioxide-rich $Ba_6Ti_{17}O_{40}$ phase, or the hexagonal $BaTiO_3$ phase.[8] We compare the behavior of the site distribution with that which is expected from the known $BaTiO_3$ defect chemistry to make tentative site assignments. We also show that dramatic changes can occur in the site distributions, even for materials prepared under the same conditions. The major site is assigned as an erbium ion substituted on a barium site that is locally charge compensated by a barium vacancy. In one crystal, we observed a very different site distribution that was assigned to locally compensated erbium ions on titanium sites. These assignments are compatible with previous work, which shows that erbium substitutes on the barium site if the dopant concentrations are low and if the Sr/Ti ratio is <1.[9,10] Previous work has also shown that erbium can substitute on the titanium site under certain conditions and that self-compensation is possible.[11]

Barium titanate is an important material for many electrooptical applications because it is a ferroelectric with interesting nonlinear and electrooptic properties.[12] When it is doped with trivalent lanthanide elements, it becomes optically active because the lanthanide ions have sharp-lined transitions between different electronic states within the unfilled $4f^n$ electron shell. In particular, erbium-doped barium titanate has been studied for use in optical waveguides, optical amplifiers, electrooptic modulators, and devices in integrated optics applications because of its strong infrared transition at 1.5 μ.[12] Erbium-doped barium titanate has also recently been studied for use in dielectrics of

* Corresponding author.

10.1021/jp053032n CCC: $30.25
Published on Web 09/13/2005

multilayer ceramic capacitors with base metal electrodes because of its excellent dielectric properties and the improved reproducibility of the materials.[11,13−16]

$BaTiO_3$ Defect Chemistry. Barium titanate is a perovskite with a point defect chemistry that depends on barium, titanium, and oxygen vacancies as well as electrons and holes. Erbium-doped barium titanate was chosen as a model system for the initial studies of barium titanate. The size of the trivalent erbium ion allows it to enter the barium titanate lattice on either a divalent barium site as a donor dopant, a tetravalent titanium site as an acceptor dopant, or both sites simultaneously, forming a self-compensating set of defects.[17] Smaller ions, such as Sc^{3+}, enter more favorably on titanium sites as acceptors, and larger ions, such as La^{3+}, enter more favorably on barium sites as donors.[11] Er^{3+} ions enter on barium sites at low dopant concentrations until the concentration exceeds the solubility on the barium site.[9,10] Er^{3+} then enters on titanium sites, where it has a higher solubility. The Ba/Ti ratio also affects the Er^{3+} site. For Ba/Ti > 1, it enters on the titanium site, and for Ba/Ti < 1, it enters on the barium site.[9,10,17] In addition, there have been suggestions that erbium can enter as a divalent ion.[14] Erbium incorporation on barium or titanium sites introduces a charge mismatch with the lattice (an aliovalent dopant) that must be charge compensated to achieve overall neutrality. The charge compensation can either be distant, in which case it contributes to the material's transport properties, or local, in which case it is trapped.

Because there are a range of possible lattice sites, it is important to examine all possible charge compensation mechanisms. The nature of the erbium charge-compensating defects can be described by Kröger and Vink notation.[18] For perovskites such as $BaTiO_3$, the lattice defects are Schottky pairs of cation and anion vacancies because interstitials cost the lattice too much energy with its closely packed structure.[1,2,19,20] For erbium substituting on a barium site, the simplest charge compensation options include the following[21]:

$$Er_2O_3 + 2TiO_2 \rightleftharpoons 2Er_{Ba}^{\bullet} + 2Ti_{Ti}^{x} + 6O_O^{x} + \frac{1}{2}O_2 + 2e' \quad (1)$$

$$Er_2O_3 + 2TiO_2 \rightleftharpoons 2Er_{Ba}^{x} + 2Ti_{Ti}^{x} + 6O_O^{x} + \frac{1}{2}O_2 \quad (2)$$

$$Er_2O_3 + 3TiO_2 \rightleftharpoons 2Er_{Ba}^{\bullet} + 3Ti_{Ti}^{x} + V_{Ba}'' + 9O_O^{x} \quad (3)$$

$$Er_2O_3 + 3TiO_2 \rightleftharpoons 2Er_{Ba}^{\bullet} + \frac{3}{2}Ti_{Ti}^{x} + 6O_O^{x} + \frac{1}{2}V_{Ti}'''' \quad (4)$$

Here, Er^{3+} is compensated by an electron in eq 1, a Ba vacancy in eq 3, and a Ti vacancy in eq 4. The Er^{2+} in eq 2 does not require charge compensation.

For erbium substituting on a titanium site,

$$Er_2O_3 + 2\,BaO \rightleftharpoons 2Ba_{Ba}^{x} + 2Er_{Ti}' + 5O_O^{x} + V_O^{\bullet\bullet} \quad (5)$$

therefore, the Er_{Ti}' is compensated by an oxygen vacancy. For erbium substituting on both a barium and titanium site,

$$Er_2O_3 \rightleftharpoons Er_{Ba}^{\bullet} + Er_{Ti}' + 3O_O^{x} \quad (6)$$

and the Er^{3+} is self-compensated. One can also transfer Er^{3+} between sites using

$$Er_{Ba}^{\bullet} + V_{Ti}'''' \rightleftharpoons Er_{Ti}' + V_{Ba}'' \quad (7)$$

In addition to the Er^{3+} equilibria, one must also consider the intrinsic Schottky defect reaction between cation and anion vacancies, the equilibria between the electronic defects and the surrounding atmosphere, and the intrinsic autoionization of electronic defects of $BaTiO_3$. At high temperatures, the electron and valance band holes are free, but, at low temperatures, electrons are likely to be localized as Ti_{Ti}', and holes are likely to be localized as $O_O^{\bullet}$.

$$BaTiO_3 \rightleftharpoons V_{Ba}'' + V_{Ti}'''' + 3V_O^{\bullet\bullet} \quad (8)$$

$$O_O^{x} \rightleftharpoons \frac{1}{2}O_2 + V_O^{\bullet\bullet} + 2e' \quad (9)$$

$$\text{nil} \rightleftharpoons Ti_{Ti}' + O_O^{\bullet} \quad (10)$$

Because the samples for this experiment were grown in a TiO_2 flux, we can also show the flux inclusion in the sample as

$$TiO_2 \rightleftharpoons V_{Ba}'' + V_O^{\bullet\bullet} + Ti_{Ti}^{x} + 2O_O^{x} \quad (11)$$

In addition to these intrinsic defect equilibria, one must also consider the effects of pairing and clustering between defects. The simplest pairing equilibria are

$$Er_{Ba}^{\bullet} + V_{Ba}'' \rightleftharpoons (Er_{Ba}^{\bullet}\cdot V_{Ba}'')' \quad (12)$$

$$Er_{Ba}^{\bullet} + V_{Ti}''' \rightleftharpoons (Er_{Ba}^{\bullet}\cdot V_{Ti}''')'' \quad (13)$$

$$Er_{Ba}^{\bullet} + V_{Ti}'''' \rightleftharpoons (Er_{Ba}^{\bullet}\cdot V_{Ti}'''')''' \quad (14)$$

$$Er_{Ba}^{\bullet} + V_{Ba}'' + O_O^{\bullet} \rightleftharpoons (Er_{Ba}^{\bullet}\cdot V_{BA}''\cdot O_O^{\bullet})^{x} \quad (15)$$

$$Er_{Ba}^{\bullet} + Ti_{Ti}' \rightleftharpoons (Er_{Ba}^{\bullet}\cdot Ti_{Ti}')^{x} \quad (16)$$

$$Er_{Ti}' + V_O^{\bullet\bullet} \rightleftharpoons (Er_{Ti}'\cdot V_O^{\bullet\bullet})^{\bullet} \quad (17)$$

$$Er_{Ti}' + V_O^{\bullet} \rightleftharpoons (Er_{Ti}'\cdot O_O^{\bullet})^{x} \quad (18)$$

Equations 16 and 18 represent the pairing of Er^{3+} with electrons or holes that are localized on Ti or O sites, respectively. Equation 15 represents a more complex center in which the local $(Er_{Ba}^{\bullet}\cdot V_{Ba}'')'$ is neutralized by a hole. Note also that pairings such as that in eq 12 result in $Er_{Ba}^{\bullet}$ and $(Er_{Ba}^{\bullet}\cdot V_{Ba}'')'$ defect structures that self-compensate each other. Pairing is important for site-selective spectroscopy because the paired and distantly compensated Er^{3+} sites are spectrally resolved, and their ratio serves as a measure of the free compensating defects which is analogous to the ratio of the protonated-to-unprotonated acid/base indicators serving as a measure of the solution pH.[22] Measurements of bulk properties probe the defect chemistry of unassociated defects, whereas site-selective spectroscopy and electron paramagnetic resonance (EPR) measurements are sensitive to locally compensated defect associations. Acceptor defect associations with oxygen vacancies[23] and valence band holes that are localized on an oxygen atom ($O_O^{\bullet}$) form pairs with alkali metal ions on barium sites.[24] Electrons localized on titanium sites (Ti_{Ti}') form pairs with oxygen vacancies and rare earth dopants.[25]

Defect equilibria are treated quantitatively in a manner identical to traditional solution equilibria; therefore, charge balance, mass balance, nonideality corrections, and equilibrium

constants describe the defect populations.[26] The system of equations can be solved simultaneously to provide the defect concentrations of all the species as a function of the dopant concentrations, oxygen partial pressure (P_{O_2}), and temperature. In this paper, we neglect activity effects.

The description of donor dopants requires consideration of the relationship between electrons (eq 1) and cation vacancies (eqs 3 and 4)[26] because electronic compensation dominates at low donor concentrations and cation compensation dominates at high donor concentrations.[23] The equilibria can be written as either

$$(V_{Ti}'''',O_O^x)'''' \rightleftharpoons (V_{Ti}'''',O_O^\bullet)''' + e' \tag{19}$$

or

$$V_{Ti}'''' \rightleftharpoons V_{Ti}''' + e' \tag{20}$$

The latter is equivalent to the ionization of a titanium vacancy. High donor dopant concentrations create V_{Ti}'''', which ionizes at high temperature. The switch from electronic to cation vacancy compensation occurs when the concentration of ionized V_{Ti}'''' exceeds the electron concentration so that the electrons are trapped by the V_{Ti}'''' as the temperature is lowered to room temperature. Typically this change occurs at 0.5 mol %, but it depends on dopants and growth conditions.[23,27]

Erbium Ion Spectra. The sharp-lined fluorescence and excitation transitions in Er^{3+} occur between partially filled $4f^{11}$ crystal fields of the local environment, and their positions and intensities are a fingerprint for the local crystal environment. At cryogenic temperatures, where only the lowest energy state is populated, the absorption spectra for transitions to a $^{2S+1}L_J$ manifold of crystal field states will have $(J + 1/2)$ lines and forced electric dipole transitions for all sites that are not cubic. For erbium's $^4S_{3/2}$ state, one expects two crystal field levels, and for the $^4I_{13/2}$ state, one expects seven. Although barium titanate is rhombohedral at 10 K, the distortion from cubic symmetry is small; therefore, erbium ions on either titanium or barium sites with distant charge compensation should have electric dipole forbidden transitions and a single-crystal field level for erbium's $^4S_{3/2}$ state (Although the rhombohedral symmetry may create a small splitting or weak transitions).[28]

Experimental Section

Crystals of barium titanate were grown from barium carbonate (Spex TMI-15 or Prochem; 99.999%) in a titanium dioxide (Aldrich or ProChem; 99.999%) flux. A mixture of 60 mol % Ti and 40 mol % Ba plus dopant ions was made. Dopants were added as oxides or nitrates (erbium: Er_2O_3, ROC/RIC 99.9%; scandium: $Sc(NO_3)_3$, ROC/RIC 99.9%; lanthanum: La_2O_3, Spex TMI-10). All dopant percentages were calculated with respect to the amount of barium ion added to the flux. The mixture was placed in a platinum crucible, which was then placed inside a block of thermal insulator to stabilize the sample temperature and heated in a programmable furnace capable of reaching 1700 °C. (Lindberg type 4434). The mixture was heated to 1500 °C and held for 6 h. One of two possible temperature programs was used. In the first, the mixture was cooled at 10 °C/hour to 900 °C. In the other it was quickly cooled to 1380 °C, held for 48 h, and then cooled at 25 °C/hour to 900 °C. The second method gave larger crystals, and these were the crystals used for this paper. Once the $BaTiO_3$ crystals were extracted from the flux, they were washed with hot sulfuric acid with extra sulfate added to increase the boiling point.

Erbium-doped crystals were grown with 0.2 mol % Er with respect to Ba. Crystals codoped with erbium and scandium were grown in an attempt to enhance the $Er_{Ba}^\bullet$ site because $Er_{Ba}^\bullet$ will compensate the Sc_{Ti}' site. These crystals consisted of 0.1 mol % Er and 0.4 mol % Sc in the flux mixture. Similarly, erbium and lanthanum-codoped crystals were grown to encourage the formation of the Er_{Ti}' site that would compensate the $La_{Ba}^\bullet$ site. These crystals consisted of 0.1 mol % Er and 0.2 mol % La in the flux mixture.

Controlled atmosphere experiments were performed by flowing CO and CO_2 gas through the furnace while annealing the samples in a platinum holder. The equilibrium between these gases controls the oxygen partial pressure through the equilibrium

$$2CO + O_2 \rightleftharpoons 2CO_2 \tag{21}$$

The ratio of the gases was controlled by flowmeters and gave $P_{O_2} \approx 10^{-16}$ atm. Experiments were performed to see which spectroscopic sites could be affected by temperature and atmospheric conditions. The samples were first examined spectroscopically and then annealed in air at 800 °C for 3 days. They were examined again to see if the fluorescence patterns had changed. They were then annealed in a 10:1 CO/CO_2 ratio atmosphere at 800 °C for 6 h and reexamined spectroscopically. Next, they were annealed in air again at 800 °C for 3 days and examined spectroscopically to determine whether the changes at low P_{O_2} were reversible. Next, they were annealed at 1250 °C in air for 24 h so that the effects of cation motion on the spectra could be observed. Finally, in an attempt to get the cation distribution of the lowest possible temperature, an extended anneal was done in which the crystals were heated to 1250 °C, and the temperature was then slowly lowered over the course of 30 days to 800 °C.

Site-selective laser spectroscopy was performed with a tunable pulsed nitrogen laser-excited dye laser with a bandwidth of ~0.5 cm^{-1} and a pulse width of ~10 ns. Nonselective fluorescence excitation scans were performed in which the dye laser wavelength was scanned, and all the fluorescence from the sample was monitored using a mechanical chopper to block the laser scatter while passing the fluorescence after a delay. Fluorescence spectra were collected using a 1-m monochromator and photomultiplier while the dye laser wavelength was held constant. Site-selective fluorescence excitation spectra could be taken by setting the 1-m monochromator at a particular wavelength and scanning the dye laser wavelength.

Samples were cooled to approximately 12 K in a cryogenic refrigerator while the spectra were collected. Fluorescence wavelengths were calibrated against Fe/Ne hollow cathode lamp emission lines. We calibrated the excitation wavelengths by splitting off a small amount of the excitation beam and measuring the Fe/Ne hollow cathode lamp's optogalvanic effect while measuring the fluorescence excitation spectra. Erbium fluorescence was monitored from the $^4S_{3/2}$ to the $^4I_{13/2}$ level after excitation from the $^4I_{15/2}$ ground state to the $^4S_{3/2}$ excited state.

Results

Er^{3+} ions in a well-defined crystallographic site have unique excitation and fluorescence spectra; therefore, the sites can be classified into spectroscopically distinguishable sites that are arbitrarily labeled. The site distribution changes caused by different doping ions, dopant concentrations, temperature, annealing atmosphere, and pressure[3,22,29] all provide information about the defect equilibria and the identity of the different sites.

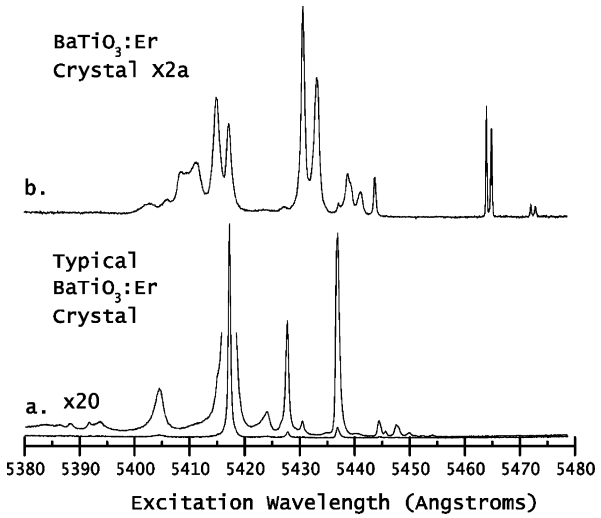

Figure 1. Nonselective Excitation Scan of BaTiO3:Er. (a) Spectrum characteristic of the three BaTiO3:Er crystals in both batches. Spectra have a ×20 expanded scale relative to panel b. (b) BaTiO3:Er crystal X2a.

Studies of the site distribution proceeded in three steps. In the first step, we measured nonselective excitation spectra, in which the wavelength of the excitation laser is scanned, and the intensity of all fluorescence is measured. This procedure identifies the absorption transitions from sites that fluoresce. The excitation spectrum of the Er^{3+} $^4S_{3/2}$ manifold was probed in four crystals from two different batches. Although the preparation conditions for the two batches were identical, the crystals from the first batch were a pink/orange color, whereas the crystals from the second batch were light yellow/brown. Despite the differences in color, the site-selective spectra for three of the crystals were very similar. The spectra of the crystal labeled X3b represents these crystals in this paper. A single Er^{3+} site (labeled the A site) dominated the spectra, but there were also several minor sites present. The fourth crystal (labeled X2a) was taken from the first batch, and it was lighter in color than the others. This crystal had a very different spectrum, as can be seen in Figure 1. Its spectrum had weak lines from the A site, but it also had lines from five other sites that were equally or more important.

In the next step, we measured the high-resolution fluorescence spectra for the $^4S_{3/2}$ to $^4I_{13/2}$ transition with the laser wavelength set on a line in the excitation spectrum that selectively excites an Er^{3+} site. The excitation nonradiatively decays to the lowest $^4S_{3/2}$ crystal field level before fluorescence occurs. The site fluorescence branching ratios determine the relative intensities of the fluorescence peaks. Fluorescence lines that have constant relative intensities are assigned to the same site. The excitation and fluorescence lines compiled in Table 1 characterize the different sites because they have minimal overlap with other sites. Examples of the fluorescence spectra from each site are shown in Figure 2.

In the third step, we measured single-site excitation spectra by scanning the dye laser while monitoring the intensity of an individual site fluorescence line. These spectra enhance the absorption features of a particular site and discriminate against those of other sites. Figure 3 shows the single-site excitation of the sites. Interfering lines from the overlapping fluorescence of other sites are labeled with an asterisk (*).

Sites C through G were only found in the crystal X2a. The spectra involving the $^4S_{3/2}$ and $^4I_{13/2}$ states of sites F and G have similar mean positions and splitting patterns, suggesting that the sites are also similar. The $^4S_{3/2}$ manifold splitting is 112 cm^{-1} and 106 cm^{-1} for the F and G sites, respectively. The C, D, and E sites are also similar, although not as similar as the F and G sites. They have $^4S_{3/2}$ splittings of 95, 99, and 98 cm^{-1}, respectively. The similarities in the fluorescence are not quite as striking as those for the F and G sites. The A site is different than the others, having the smallest splitting of the $^4S_{3/2}$ level at 70 cm^{-1}. One of the $^4S_{3/2}$ lines is so weak that it is difficult to see without scale expansion. The spectra of all the sites in crystal X2a were bright and well-resolved.

TABLE 1: Excitation and Fluorescence Wavelengths Used for Measuring Particular Er Sites

site label	excitation wavelength (nm.)	fluorescence wavelength (nm.)
A	541.71	843.71
B1	542.72	846.33
B2	542.90	845.97
B3	543.04	847.69
C	541.13	853.84
D	541.49	860.29
E	540.83	845.02
F	543.11	847.70
G	543.32	847.87
H	542.19	853.38
I	544.06	844.95
J	544.45	849.01
K	544.80	845.85
S	545.70	844.31

The A site dominated the spectra in all the remaining crystals with an intensity that was at least 20 times brighter than the other sites. Interference from spectral overlap with the A site is seen in most of the spectra for sites B and H−K. These sites were observed in all the crystals except X2a. The I and J sites were dim and obscured enough that only one $^4S_{3/2}$ absorbance line could be observed for each site. The J site fluorescence to the $^4I_{13/2}$ level showed more than the expected $J + 1/2$ lines, so it might be a cluster of two or more Er^{3+} ions that exchange energy. The H and K sites show a 20 and 11 cm^{-1} splitting, respectively, in the $^4S_{3/2}$ level. Because the H, I, J, and K sites

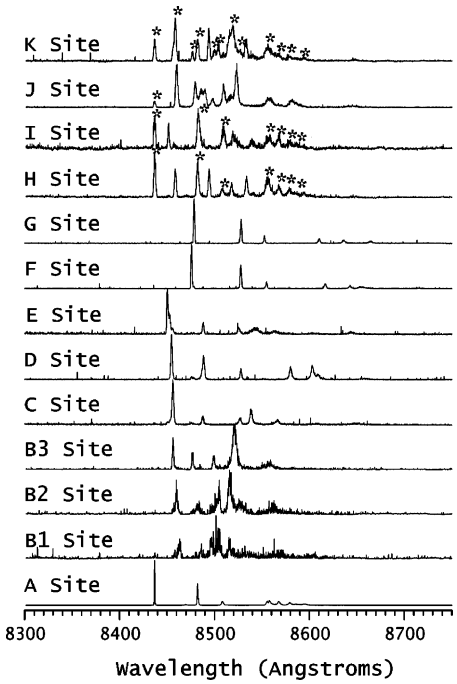

Figure 2. Fluorescence of BaTiO3:Er showing $^4S_{3/2}$ to $^4I_{13/2}$ fluorescence spectra for each erbium site. Site A is present in all crystals. Sites C−G are only present in the crystal X2a. Sites B and H−K are present in most crystals. The asterisk (*) indicates lines with interference from another site.

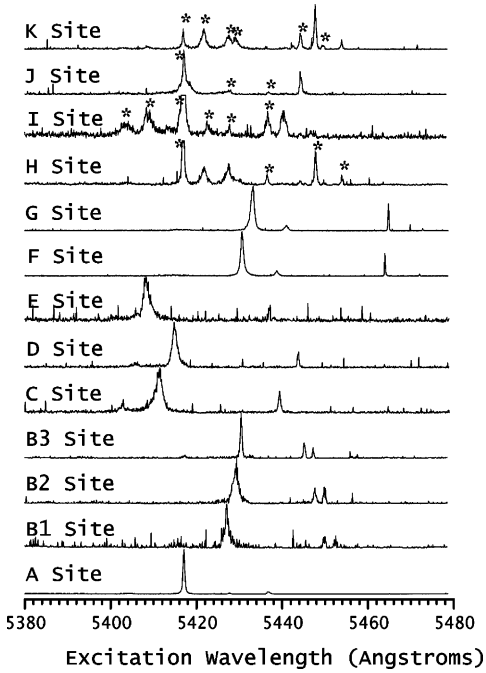

Figure 3. Site-selective spectra of erbium sites in BaTiO3:Er crystals. Sites A,B and H−K occur in most crystals, whereas sites C−G occur only in crystal X2a.

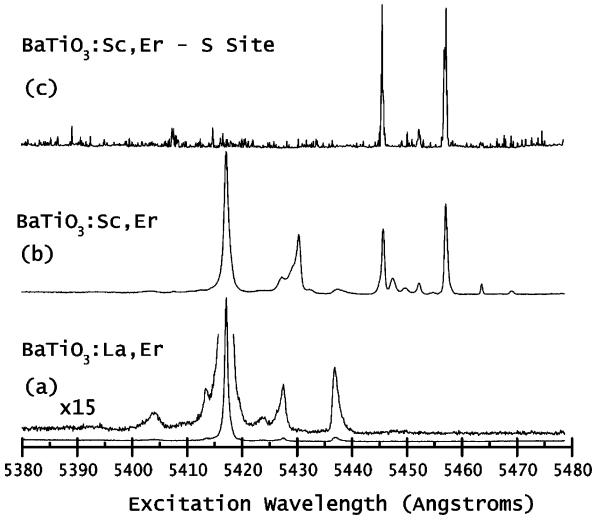

Figure 4. Nonselective excitation of doubly doped BaTiO3 crystals. $^4I_{15/2}$ to $^4S_{3/2}$ excitation scans for the codoped erbium and another dopant ion. (a) 0.2% La/0.1% Er. (b) 0.4% Sc/0.1% Er. (c) Excitation scan showing the S site in a Sc/Er crystal.

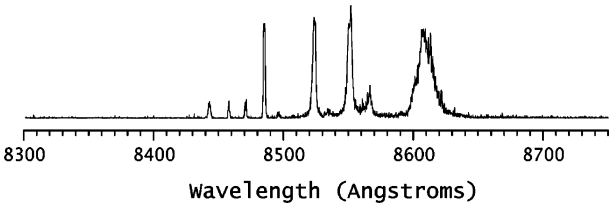

Figure 5. S Site $^4S_{3/2}$ to $^4I_{13/2}$ fluorescence. This site was only found in the erbium/scandium doubly doped crystals.

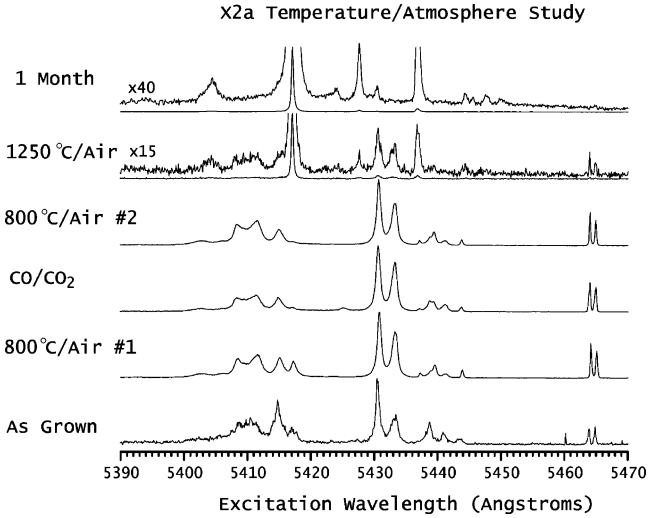

Figure 6. Temperature and atmosphere study of crystal X2a. Nonselective fluorescence from crystal X2a annealed under different conditions. (a) as grown; (b) 800 °C for 3 days in air; (c) 800 °C and $P_{O_2} = 10^{-16}$ atm in CO/CO_2 for 6 h; (d) 800 °C for 3 days; (e) 1250 °C for 24 h; and (f) 1250 °C cooled to 800 °C over 30 days.

are weak under every preparation condition, we will not discuss them further.

Once the erbium sites were characterized, the spectroscopy could follow the site distribution changes resulting from different crystal processing conditions. In this report, we used both codoping with either donor or acceptor ions and treatment of the crystals at elevated temperatures in different oxidizing or reducing atmospheres to change the defect chemistry occurring in the crystal. Lower temperatures do not allow cation motion in the crystal lattice, so changes seen in the distribution of sites are likely to be due to associations or disassociations with oxygen defects and/or electronic defects. Higher temperatures allow the cations to move as well, so changes that only occur at high temperatures are likely to be due to cation and anion vacancy motion.[30]

One set of crystals doped with both scandium and erbium was grown. They had a very pale red/brown color. Two crystals from this batch were examined, and they showed similar characteristics to the Er^{3+}-doped crystals in which the A site was dominant, but each crystal also had one additional site that we labeled the S site (Figures 4 and 5), which was not seen in other crystals. The crystals also had enhanced B1, B2, and B3 site intensities.

Another set of crystals doped with lanthanum and erbium were grown. These crystals were dark black. The site-selective spectra were dominated by transitions from the A site (see Figure 4). The dark color of the crystals absorbed sufficiently so that it was difficult to observe fluorescence from the weaker sites.

Figures 6 and 7 show the excitation spectra with broadband fluorescence monitoring for a series of annealing experiments on the X2a and X3b crystals. The first and last annealing experiments at 800 °C were intended to create the same equilibration conditions before and after the annealing at reduced P_{O_2} so one could isolate the changes caused by the reduced P_{O_2}. Comparing these excitation spectra with the spectra of the "as-grown" crystal shows small changes in the relative site concentrations for the X3B crystals and very large changes in the X2a crystal. Table 2 summarizes the peak height intensities relative to the as-grown sample after the intensities were normalized to the most intense peak in each spectrum.

In crystal X3b, the first annealing in air at 800 °C changed only the H site intensity to a lower value relative to the as-grown condition. Annealing in a reducing CO/CO_2 mixture caused small increases in the B3, I, and J sites. The second annealing in air at 800 °C caused small decreases in the B2, B3, H, and J sites. Further annealing in air at 1250 °C caused an increase in the B3 and J sites and a decrease in the H site. After 1 month of annealing at 1250 °C, the B3 and H sites

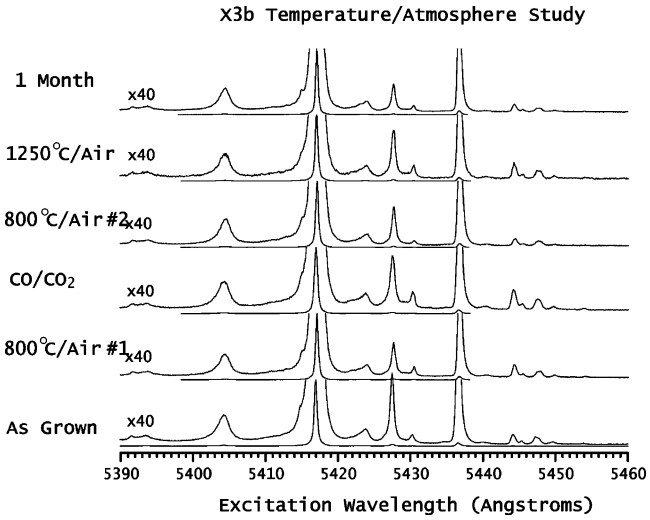

Figure 7. Temperature and atmosphere study of crystal X3b. Nonselective fluorescence from crystal X3b annealed under different conditions. (a) as grown; (b) 800 °C for 3 days in air; (c) 800 °C and $P_{O_2} = 10-16$ atm in CO/CO_2 for 6 h; (d) 800 °C for 3 days; (e) 1250 °C for 24 h; and (f) 1250 °C cooled to 800 °C over 30 days.

TABLE 2: Ratios of Er Site Peak Intensities under Different Preparation Conditions

site intensity ratios	0.4% Sc^{3+}, 0.1% Er^{3+}	0.2% Er^{3+}	0.2% La^{3+}, 0.1% Er^{3+}
B1/A	0.068	0.027	0.024
B2/A	0.17	<.002	0.002
B3/A	0.25	0.004	<.002

site	as grown	air, 800 °C (#1)	CO/CO_2, 800 °C	air, 800 °C (#2)	1250 °C	1250 →800 °C over 1month
			Crystal X2a			
A	1	1	0.29	0.02	3.7	1[a]
B1						
B2						4.7[a]
B3						7.3[a]
C	1	0.90	0.63	0.93	0.05	
D	1	0.47	0.33	0.37	0.04	
E	1	0.88	0.64	0.94	0.07	
F	1	1	1	1	0.05	
G	1	1.5	1.6	1.4	0.08	
H					1.2[a]	0.86[a]
I						
J						0.93[a]
K						
			Crystal X3b			
A	1	1	1	1	1	1
B1	1	1	1	1	1	1
B2	1	1	1	0.25	1	1
B3	1	1	2.3	0.38	1.7	0.87
H	1	0.47	0.74	0.54	0.67	0.37
I	1	1	4.3	1	1	1
J	1	1	2.1	0.72	1.7	0.76
K	1	1	1	1	1	0

[a] Ratio calculated using as-grown X3b.

decreased and the K site vanished, but the other sites did not change appreciably. The increases of the B3, I, and J sites in a reducing atmosphere suggests that these sites increase when the electron or oxygen vacancy concentrations increase. The I site is unusual in that low partial pressures of oxygen in CO/CO_2 cause large increases in concentration, but no changes occur from the as-grown state under any other condition. The B1 site maintains a constant ratio with the A site under all conditions, and the B2 site only responded to the second low-temperature anneal in air and then returned to its as-grown state.

In crystal X2a, the F site remained the brightest site at lower temperatures. The spectral intensity of the G site rose somewhat compared to that of the F site. The site intensities of the A and D sites consistently diminished during lower-temperature annealing. The C and E sites diminished when annealed in CO/CO_2 but recovered on their second anneal in air at 800 °C. As soon as the crystal was annealed at 1250 °C, a significant change in the site distribution occurred, and the A site became dominant. After being annealed for 30 days, the crystal converted to a site distribution that was indistinguishable from the other crystals. The C, D, E, F, and G sites disappeared and B2, B3, H, and J sites appeared. The crystal also visibly darkened, showing an increase in the number of electrons compensating the defects in the crystal.

Point Defect Equilibrium Calculations. To correlate the changes in the site distribution with the point defect equilibria, we calculated the expected point defect concentrations using the equilibrium constants from the literature for the reactions discussed earlier in this paper.[26] The mass action relationships and the associated equilibrium constants are summarized in Table 3. The value of K_{FL} was calculated from the data of Yoon and Kim.[26] They used the $[V''_{Ba}]/[Ti'''_{Ti}]$ ratio as an adjustable fitting parameter. This ratio is related to $V_O^{\bullet\bullet}$ by

$$\frac{[V''_{Ba}]}{[V_{Ti}^{Tot}]} = \frac{[V_O^{\bullet\bullet}]a_{TiO_2}{}^2 K_{FL}{}^2}{K_S} \tag{22}$$

A value for K_{FL} was found by fitting it to the critical donor concentration for the semiconducting to insulating transition. Yoon and Kim found critical concentrations for annealing in air of 2.0−2.3 mol % at 1400 °C, 1.2−1.4 mol % at 1200 °C, and ∼0.5 mol % when slowly cooled to 1000 °C. This critical donor concentration occurs when the $[V'''_{Ti}]$ exceeds $[n']$; therefore, all the electrons would be trapped by the partially ionized titanium vacancies upon being cooled, leaving the material as an insulator. This estimate provided the value given in Table 3.

We estimated the equilibrium constants for defect pairing with the erbium dopant from our data using the arguments presented in the discussion. The estimates are summarized in Table 3. For a pairing equilibrium between $Er^{\bullet}_{Ba}$ and a charge compensation, L_n, one can write

$$K_n = \frac{[(Er^{\bullet}_{Ba}\cdot L_n)]}{[Er^{\bullet}_{Ba}][L_n]} \tag{23}$$

therefore, the fraction of the erbium concentration, C_{Er}, that is associated with a particular local charge compensation, $(Er^{\bullet}_{Ba}\cdot L_n)$, can be written as

$$\alpha_n = \frac{K_n[L_n]}{1 + \sum_i K_i[L_i]} C_{Er} \tag{24}$$

The equilibrium between $Er^{\bullet}_{Ba}$ and Er'_{Ti} sites depends on the cation vacancy ratio (see eq 7) because

$$K_{Er} = \frac{[Er^{\bullet}_{Ba}][V''_{Ti}]}{[Er'_{Ti}][V^{*}_{Ba}]} = \frac{[Er^{\bullet}_{Ba}]}{[Er'^{\circ}_{Ti}]} \frac{K_s}{K_{FL}^2 [V_O^{\bullet\bullet}] a_{TiO_2}^2} \tag{25}$$

The high $[V_O^{\bullet\bullet}]$ that occurs from acceptor doping favors $Er^{\bullet}_{Ba}$, whereas the low $[V_O^{\bullet\bullet}]$ that occurs from donor doping favors

TABLE 3: Mass Action Relationships and Equilibrium Constants Used to Model the Defect Equilibria[a]

equilibrium expression	K at 1350 °C and $P_{O_2} = 0.2$
$K_S = [V''_{Ba}][V_{Ti}^{Tot}][V_O^{\bullet\bullet}]^3 = 10^{116}\exp\left(\frac{-10.5eV}{kT}\right)\text{cm}^{-15}$	$2 \times 10^{83}\ \text{cm}^{-15}$
$K_O = [V_O^{\bullet\bullet}][Ti'_{Ti}]^2 P_{O_2}{}^{(1/2)} = 2.56 \times 10^{71}\exp\left(\frac{-6.1eV}{kT}\right)\text{cm}^{-9}\,\text{atm}^{-(1/2)}$	$3 \times 10^{52}\ \text{cm}^{-9}\ \text{atm}^{-1/2}$
$K_i = [Ti'_{Ti}]\cdot[O_O^{\bullet}] = 10^{45}\exp\left(\frac{-2.9eV}{kT}\right)\text{cm}^{-6}$	$10^{36}\ \text{cm}^{-6}$
$K_{FL} = \frac{[V''_{Ba}][V_O^{\bullet\bullet}]}{a_{TiO_2}} = 7.1 \times 10^{43}\exp\left(\frac{-3.02eV}{kT}\right)\text{cm}^{-6}$	$3 \times 10^{34}\ \text{cm}^{-6}$
$K_{Ti} = \frac{[V''''_{Ti}][Ti'_{Ti}]}{[V''''_{Ti}]} = 1.6 \times 10^{22}\exp\left(\frac{-1.14eV}{kT}\right)\text{cm}^{-3}$	$5 \times 10^{18}\ \text{cm}^{-3}$
$K = \frac{[(Er_{Ba}^{\bullet}\cdot V''_{Ba})']}{[Er_{Ba}^{\bullet}][V''_{Ba}]}$	$9 \times 10^{-20}\ \text{cm}^3$
$K = \frac{[(Er_{Ba}^{\bullet}\cdot V''''_{Ti})'''']}{[Er_{Ba}^{\bullet}][V''''_{Ti}]}$	$2 \times 10^{-21}\ \text{cm}^3$
$K = \frac{[(Er_{Ba}^{\bullet}\cdot Ti'_{Ti})^x]}{[Er_{Ba}^{\bullet}][Ti'_{Ti}]}$	$7 \times 10^{-22}\ \text{cm}^3$
$K = \frac{[(Er_{Ba}^{\bullet}\cdot V''_{Ba}\cdot O_O^{\bullet})^x]}{[Er_{Ba}^{\bullet}][V''_{Ba}][O_O^{\bullet}]}$	$10^{-39}\ \text{cm}^6$
$K = \frac{[(Er_{Ba}{}^{\bullet}\cdot V_O^{\bullet\bullet})^{\bullet}]}{[Er'_{Ti}][V_O^{\bullet\bullet}]}$	$2 \times 10^{-20}\ \text{cm}^3$
$K = \frac{[(Er'_{Ti}\cdot O_O^{\bullet})^x]}{[Er'_{Ti}][O_O^{\bullet}]}$	$10^{-20}\ \text{cm}^3$
$K = \frac{[Er_{Ba}^{\bullet}][V''''_{Ti}]}{[Er'_{Ti}][V''_{Ba}]}$	10^2

[a] The constants for the erbium defect equilibria were chosen to match spectral intensities rather than site concentrations.

Er'_{Ti}. If $C_{Er_{Ti}}$ and $C_{Er_{Ba}}$ are the total concentrations of erbium on either lattice site, one can write

$$C_{Er_{Ti}} = \frac{\alpha_{Er_{Ba}^{\bullet}} K_s}{\alpha_{Er_{Ba}^{\bullet}} K_s + \alpha_{Er'_{Ti}} K_{Er} K_{FL}{}^2 [V_O^{\bullet\bullet}]} C_{Er} \quad (26)$$

$$C_{Er_{Ba}} = \frac{\alpha_{Er'_{Ti}} K_{Er} K_{FL}{}^2 [V_O^{\bullet\bullet}]}{\alpha_{Er_{Ba}^{\bullet}} K_s + \alpha_{Er'_{Ti} K_{Er} K_{FL}{}^2 [V_O^{\bullet\bullet}]}} C_{Er} \quad (27)$$

The charge balance for a system that is doped with Er^{3+}, La^{3+}, and/or Sc^{3+} is

$$2[V_O^{\bullet\bullet}] + [Er_{Ba}^{\bullet}] + [(Er'_{Ti}\cdot V_O^{\bullet\bullet})^{\bullet}] + [La_{Ba}^{\bullet}] + p^{\bullet} = 2[V''_{Ba}] + 3[V''''_{Ti}] + 4[V''''_{Ti}] + [Er'_{Ti}] + [(Er_{Ba}^{\bullet}\cdot V''_{Ba})'] + [(Er_{Ba}^{\bullet}\cdot V''''_{Ti})''] + [Sc'_{Ti}] + n' \quad (28)$$

Substituting the mass action relationships then gives

$$\frac{2K_O}{[n]^2\sqrt{P_{O_2}}} + [Er_{Ba}^{\bullet}] + [(Er'_{Ti}\cdot V_O^{\bullet\bullet})^{\bullet}] + [La_{Ba}^{\bullet}] + \frac{K_i}{[n]} = \frac{2[n]^2 K_{FL}\sqrt{P_{O_2}}}{K_O} + \frac{[n]^4 K_s P_{O_2}}{K_{FL} K_O{}^2}\left\{4 - \left[1 + \frac{N_C}{n}\exp(E(V''''_{Ti}))\right]^{-1}\right\} + [Er'_{Ti}] + [(Er_{Ba}^{\bullet}\cdot V''_{Ba})'] + [(Er_{Ba}^{\bullet}\cdot V''''_{Ti})''] + [Sc'_{Ti}] + [n] \quad (29)$$

This equation can be numerically solved for the electron concentration in terms of P_{O_2}, temperature, and dopant concentrations. The concentrations of all other species then follow. Figure 8a shows the simulation for the concentrations of all the intrinsic point defects over a range of donor and acceptor concentrations, whereas Figure 8b shows the concentrations of the erbium sites. The simulation assumed an erbium concentration of 0.1 mol %, an equilibration temperature of 1350 °C, and $P_{O_2} = 0.2$.

Discussion

Erbium can enter the $BaTiO_3$ lattice on either barium or titanium sites; therefore, if erbium was not paired with a defect charge compensation, the spectrum could contain only 2 sites. Although barium titanate is rhombohedral at our measurement temperatures, it remains cubic to a good approximation, so we do not expect to see either of these sites in the spectrum. The 13 sites we do see have a lower symmetry that is caused by local charge compensation. The simulations in Figure 8 show that the intrinsic defect concentrations change by between 2 and 10 orders of magnitude over the range of dopant concentrations in this study. The spectral changes observed in Figures 1 and 4 are smaller because the spectra reflect the relative changes in the erbium site distributions. The interpretation of the site concentrations rests on several observations. First, the A site is the dominant site throughout the range of dopants from the Sc^{3+}- to the La^{3+}-doped crystals. Second, the color of the crystals became markedly lighter in the Sc^{3+}-doped crystal, reflecting a change from electron to hole dominance. In addition, the site distribution of the Er^{3+}:$BaTiO_3$ crystals reflected in the spectrum of Figure 1 was very similar to that of the La^{3+},Er^{3+}:$BaTiO_3$

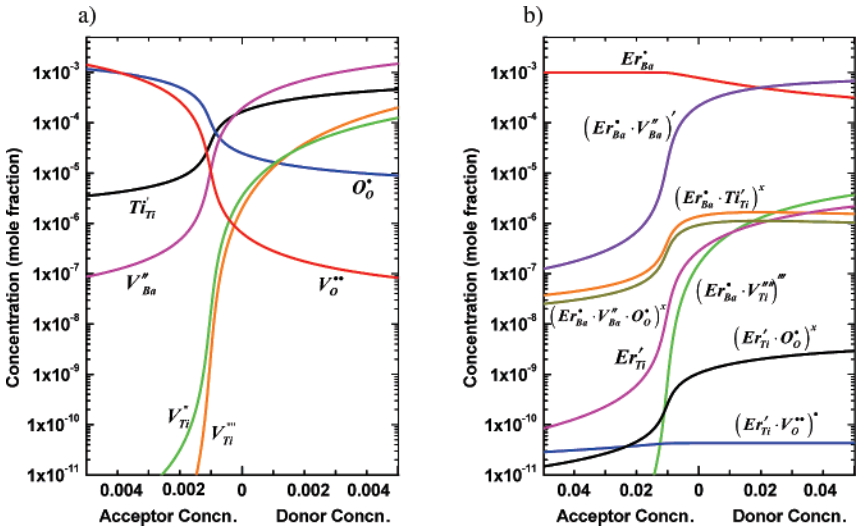

Figure 8. Simulations of the defect equilibria as a function of the concentrations of either donor or acceptor dopants (mole fraction) using the parameters defined in Table 3. The simulations assume the erbium concentration is 0.1 mol %, the P_{O_2} is 0.2 atm, and the equilibrium temperature is 1350 °C. (a) Intrinsic defect concentrations. (b) Erbium site concentrations.

TABLE 4: Dependence of the Concentration of the Different Er^{3+} Centers on the Dominant Charge Compensation Concentration[a]

	$Er^{\bullet}_{Ba}$ & V''_{Ba} dominant	Er'_{Ti} & $V^{\bullet\bullet}_{O}$ dominant
$Er^{\bullet}_{Ba}$		$[V^{\bullet\bullet}_{O}]$
$(Er^{\bullet}_{Ba}\cdot V''_{Ba})'$	$[V''_{Ba}]$	
$(Er^{\bullet}_{Ba}\cdot V''''_{Ti})''''$	$[V''_{Ba}]^2$	$1/[V^{\bullet\bullet}_{O}]$
$(Er^{\bullet}_{Ba}\cdot Ti'_{Ti})^{x}$	$\sqrt{[V''_{Ba}]}/P_{O_2}{}^{1/4}$	$\sqrt{[V^{\bullet\bullet}_{O}]}/P_{O_2}{}^{1/4}$
$(Er^{\bullet}_{Ba}\cdot V''_{Ba}\cdot O^{\bullet}_{O})^{x}$	$\sqrt{[V''_{Ba}]}P_{O_2}{}^{1/4}$	$\sqrt{[V^{\bullet\bullet}_{O}]}P_{O_2}{}^{1/4}$
Er'_{Ti}	$[V''_{Ba}]$	
$(Er'_{Ti}\cdot V^{\bullet\bullet}_{O})^{\bullet}$		$[V^{\bullet\bullet}_{O}]$
$(Er'_{Ti}\cdot O^{\bullet}_{O})^{x}$	$\sqrt{[V''_{Ba}]}P_{O_2}{}^{1/4}$	$\sqrt{[V^{\bullet\bullet}_{O}]}\,P_{O_2}{}^{1/4}$

[a] Assuming erbium enters lattice on either the titanium or barium sites.

crystal and less similar to that of the Sc^{3+},Er^{3+}:$BaTiO_3$ crystal. Both of these observations suggest the Er^{3+} enters the lattice on a barium site and acts as a donor dopant. Third, the B/A intensity ratio increases as the crystals become more dominated by $V^{\bullet\bullet}_{O}$ and $O^{\bullet}_{O}$ defects. Table 4 summarizes the dependence of each site concentration on the dominant ionic defect for the cases in which erbium enters on the barium or titanium site. The B/A increase would correlate with site ratios that increase when $[V''_{Ba}]$ decreases, if erbium enters on the barium site, or when $[V_O{}^{\bullet\bullet}]$ increases, if erbium enters on the titanium site. The exact functional dependence is defined by the simulations.

Simulations of the defect equilibria and the erbium site distribution were performed for erbium replacing either barium or titanium sites. We did not find any parameters that were consistent with the observed site intensity changes as the crystals were changed from donor to acceptor doping if we assumed the erbium entered on the titanium site. The main problem was explaining why the site ratio for the La^{3+},Er^{3+}:$BaTiO_3$ and Er^{3+}:$BaTiO_3$ crystals were similar if erbium was entering as an acceptor ion. We did find parameters that were consistent with the observed site changes if we assumed the erbium entered on the barium site. In particular, the erbium spectra would be similar for the La^{3+},Er^{3+}:$BaTiO_3$ and Er^{3+}:$BaTiO_3$ crystals if La^{3+} and Er^{3+} both entered as donor dopants. The simulation parameters for the best fit of the relative intensities are summarized in Table 3. One must remember that the K parameters for the erbium-pairing equilibria were chosen to fit

TABLE 5: Values of Site Intensity Ratios Determined by the Simulation Model with the Parameters Listed in Table 3

site intensity ratios	0.4% Sc^{3+}, 0.1% Er^{3+}	0.2% Er^{3+}	0.2% La^{3+}, 0.1% Er^{3+}
B1/A	0.04	0.04	0.04
B2/A	0.17	0.004	0.002
B3/A	0.25	0.006	0.003

line intensities, not site concentrations; therefore, these parameters cannot be taken as true equilibrium constants. The pairing parameters for the sites in which erbium occupies a titanium site were chosen to create site concentrations that were too low to affect the defect equilibria but high enough so that one could still see how the distributions of these sites change. Because we do not believe that these Er_{Ti} sites are reflected in the spectra, the values of the parameters are only illustrative.

The simulation in Figure 8 shows that the $(Er^{\bullet}_{Ba}\cdot Ti'_{Ti})^{x}$ and the $(Er^{\bullet}_{Ba}\cdot V''_{Ba}\cdot O^{\bullet}_{O})^{x}$ sites increase relative to the $(Er^{\bullet}_{Ba}\cdot V''_{Ba})'$ site as the crystal becomes more acceptor-doped. Table 5 shows that the ratio of these sites matches the observed B2/A and B3/A intensity ratios for the parameters chosen. The B1/A site ratio does not change appreciably over the range of dopant conditions, showing that the two sites have the same dependence on the intrinsic defect concentrations. The B1 site would then correspond to a different local arrangement of the erbium and the compensating barium vacancy in a $(Er^{\bullet}_{Ba}\cdot V''_{Ba})'$ center. We did not see any sites with dependences appropriate for titanium vacancy compensation, and the simulations also show that the titanium vacancy concentrations should be negligibly low.

Because the $(Er^{\bullet}_{Ba}\cdot Ti'_{Ti})^{x}$ and $(Er^{\bullet}_{Ba}\cdot V''_{Ba}\cdot O^{\bullet}_{O})^{x}$ sites have the same dependence on the intrinsic defect concentrations (see Table 4), it is not possible to distinguish between the assignments for the B2 and B3 sites from the data on the doping experiments, but one can distinguish them by the difference in their dependence on P_{O_2}. Annealing the samples at a P_{O_2} of 10^{-16} atm should change the electronic defect concentrations by 4 orders of magnitude, but the observed changes are smaller. There is a small enhancement in the concentration of the B3 site, which is not seen for the other sites. Although the enhancement may indicate the site is associated with an electronic compensation, it is not definitive evidence. Because Table 3 shows that an enhancement is expected for the $(Er^{\bullet}_{Ba}\cdot Ti'_{Ti})^{x}$ site at low P_{O_2}, we assign the B3 site to the $(Er^{\bullet}_{Ba}\cdot Ti'_{Ti})^{x}$

center and the B2 site to the $(Er^{\bullet}_{Ba}\cdot V''_{Ba}\cdot O^{\bullet}_{O})^{x}$ center but the small enhancement keeps this assignment from being definitive.

In addition to the normal sites, the Sc^{3+},Er^{3+}:$BaTiO_3$ crystal contains the S site, a site observed only for this crystal. Because it is known that scandium can only occupy the titanium site, the presence of the S site in the Sc^{3+},Er^{3+}-doped crystal strongly suggests that the S site is a $(Er^{\bullet}_{Ba}\cdot Sc'_{Ti})^{x}$ association and is further evidence for erbium entering the lattice on a barium site.[11,14,25,31] A similar example was observed when Pr^{3+}:$BaTiO_3$ was codoped with other lanthanide ions.[31]

Crystal X2a is intriguing because, although it does exhibit a very weak contribution from the A site, its other sites are different from any other crystal. Furthermore, Figure 6 shows that strong heating causes the spectra to revert to that observed for the other crystals. Clearly, the as-grown crystal is not at equilibrium, and a high temperature is required to establish the equilibrium. The metastable state of the as-grown crystal must correspond to a nonequilibrium distribution of cations and cation vacancies because high temperatures are required for equilibration. The electrons, holes, and oxygen vacancies would be mobile at the lower temperatures used in Figure 6, and no significant changes occur at those temperatures.[32] Because the site distribution of all the other crystals is dominated by the A site regardless of whether the crystal is donor-doped or acceptor-doped, and because none of the C−G sites of the X2a crystal appear in the donor- or acceptor-doped crystals, the as-grown X2a site distribution must be defined by factors that are not important in the other crystals, even though the crystals have dopants that range from acceptor to donor. Furthermore, the C−G sites must be locally compensated because their site symmetry cannot be near cubic, and the local compensations must be different from the other crystals. The most obvious explanation for the differences is that Er^{3+} is entering on the titanium site in this crystal and that high-temperature annealing can cause it to switch to the barium site. The C−G sites would then correspond to $(Er'_{Ti}\cdot V^{\bullet\bullet}_{O})^{\bullet}$, $(Er'_{Ti}\cdot V^{\bullet\bullet}_{O}\cdot Ti'_{Ti})^{x}$, and/or $(Er'_{Ti}\cdot O^{\bullet}_{O})^{x}$ sites. Substitution of erbium on a titanium site would result in an acceptor doping and produce the pale color that is characteristic of acceptor dopants. The darkening of the crystal upon conversion to the normal site distribution is consistent with the erbium substitution changing to a donor lattice position. Previous work makes it clear that Er^{3+} can enter the lattice as Er'_{Ti} under BaO-rich growth conditions; therefore, this explanation seems plausible.[9,10,11,17] Equation 31 shows that Er'_{Ti} is favored by a high $[V'''_{Ti}]$ and a low $[V^{\bullet\bullet}_{O}]$ and a_{TiO_2}, but further work is required to reproductively control erbium substitution on the titanium site and its interconversion to the barium site.

Conclusions

Site-selective spectroscopy identified 13 spectroscopically distinct sites for erbium ion in the $BaTiO_3$ lattice. Only trivalent erbium was seen; divalent erbium was not observed. The dominant site in all but one crystal was assigned as $(Er^{\bullet}_{Ba}\cdot V''_{Ba})'$ (labeled A site), regardless of whether the crystal was donor- or acceptor-doped. Three lower-intensity sites had similar spectroscopic characteristics and were labeled B1, B2, and B3. The B2/A and B3/A site ratios increase as the doping is changed from donor to acceptor, and comparison with simulations assigns them as $(Er^{\bullet}_{Ba}\cdot V''_{Ba}\cdot O^{\bullet}_{O})^{x}$ and $(Er^{\bullet}_{Ba}\cdot Ti'_{Ti})$ sites. The assignments also rely on the enhancement of the B3 site intensity in experiments performed with reduced P_{O_2}. The B1/A site ratio does not change appreciably, and B1 is assigned as an $(Er^{\bullet}_{Ba}\cdot V''_{Ba})'$ site that is crystallographically different from the A site. Sites C−G were only seen in one crystal, and these sites could be eliminated by annealing the crystal at 1250 °C. They have been tentatively identified as $(Er'_{Ti}\cdot V^{\bullet\bullet}_{O})^{\bullet}$, $(Er'_{Ti}\cdot V^{\bullet\bullet}_{O}\cdot Ti'_{Ti})^{x}$, and/or $(Er'_{Ti}\cdot O^{\bullet}_{O})^{x}$ sites where erbium enters the lattice on a titanium site. These assignments explain the observations reported in this paper, but more experiments are required to make these assignments definitive.

Acknowledgment. The authors acknowledge the National Science Foundation for their support through grant number DMR-8815398.

References and Notes

(1) Maier, J. *Angew. Chem., Int. Ed. Engl.* **1993**, *32*, 528.
(2) Maier, J. *Angew. Chem., Int. Ed. Engl.* **1993**, *32*, 313.
(3) Wright, J. C.; *Cryst. Lattice Defects Amorphous Mater.* **1985**, *12*, 505.
(4) Cockroft, N. J.; Lee, S. H.; Wright, J. C. *Phys. Rev. B: Condens. Matter* **1991**, *44*, 4117.
(5) Cockroft, N. J.; Wright, J. C. *Phys. Rev. B: Condens. Matter* **1992**, *45*, 9642.
(6) Knott, L. J.; Cockroft, N. J.; Wright, J. C. *Phys. Rev. B: Condens. Matter* **1995**, *51*, 5649.
(7) Knott, L. J.; Wright, J. C. *J. Lumin.* **1994**, *60−1*, 227.
(8) Bak, J. D.; Wright, J. C. Thesis, University of Wisconsin, 2003.
(9) Buscagliia, M. T.; Viviani, M.; Buscaglia, V.; Bottino, C. *J. Am. Ceram. Soc.* **2002**, *85*, 1569.
(10) Buscagliia, M. T.; Buscaglia, V.; Ghigna, P.; Viviani, M.; Spinolo, G.; Testino, A.; Nanni, P. *Phys. Chem. Chem. Phys.* **2004**, *6*, 3710.
(11) Tsur, Y.; Hitomi, A.; Scrymgeour, I.; Randall, C. A. *Jpn. J. Appl. Phys., Part 1* **2001**, *40*, 255.
(12) Wessels, B. W.; Block, B. A. U.S. Patent 6,122,429, 2000.
(13) Tsur, Y.; Randall, C. A. Charge Compensation in Barium Titanate. In *Applications of Ferroelectrics 2000*, Proceedings of the 2000 IEEE International Symposium on Applications of Ferroelectrics, Honolulu, HI, July 21−Aug. 2, 2000; IEEE: New York, 2000; Vol. 1, p 151.
(14) Tsur, Y.; Dunbar, T. D.; Randall, C. A. *J. Electroceram.* **2001**, *7*, 25.
(15) Tsur, Y.; Randall, C. A. *AIP Conf. Proc.* **2000**, *535*, 283.
(16) Tsur, Y.; Randall, C. A. *J. Am. Ceram. Soc.* **2001**, *84*, 2147.
(17) Takada, K.; Chang, E.; Smyth, D. M. *Adv. Ceram.* **1986**, *19*, 147.
(18) Kroger, F. A.; Vink, H. J. *Solid State Physics, Advances in Research and Applications*; Academic Press Inc.: New York, 1956; Vol. 3, p 307.
(19) Sasaki, K.; Maier, J. *J. Appl. Phys.* **1999**, *86*, 5422.
(20) Sasaki, K.; Maier, J. *J. Appl. Phys.* **1999**, *86*, 5434.
(21) Dunbar, T. D.; Warren, W. L.; Tuttle, B. A.; Randall, C. A.; Tsur, Y. *J. Phys. Chem. B* **2004**, *108*, 908.
(22) Cirillo-Penn, K. M.; Wright, J. C. *Phys. Rev. B: Condens. Matter* **1990**, *41*, 10799.
(23) Scharfschwerdt, R.; Mazur, A.; Schirmer, O. F.; Hesse, H.; Mendricks, S. *Phys. Rev. B: Condens. Matter* **1996**, *54*, 15284.
(24) Varnhorst, T.; Schirmer, O. F.; Krose, H.; Scharfschwerdt, R.; Kool, T. W. *Phys. Rev. B: Condens. Matter* **1996**, *53*, 116.
(25) Glinchuk, M. D.; Bykov, I. P.; Kornienko, S. M.; Laguta, V. V.; Slipenyuk, A. M.; Bilous, A. G.; V'yunov, O. I.; Yanchevskii, O. Z. *J. Mater. Chem.* **2000**, *10*, 941.
(26) Yoon, S. H.; Kim, H. *J. Appl. Phys.* **2002**, *92*, 1039.
(27) Jonker, G. H. *Solid-State Electron.* **1964**, *7*, 895.
(28) Tallant, D. R.; Wright, J. C. *J. Chem. Phys.* **1975**, *63*, 2075.
(29) Olsen, L. R.; Wright, A. O.; Wright, J. C. *Phys. Rev. B: Condens. Matter* **1996**, *53*, 14135.
(30) Yoo, H. I.; Lee, D. K. *Phys. Chem. Chem. Phys.* **2003**, *5*, 2212.
(31) Okamoto, S.; Yamamoto, H. *J. Appl. Phys.* **2002**, *91*, 5492.
(32) Wernicke, R. *Philips Res. Rep.* **1976**, *31*, 526.